

Weakly Supervised 3D Object Detection with Multi-Stage Generalization

Jiawei He^{1,2} Yuqi Wang^{1,2} Yuntao Chen³ Zhaoxiang Zhang^{1,2,3}

Abstract

With the rapid development of large models, the need for data has become increasingly crucial. Especially in 3D object detection, costly manual annotations have hindered further advancements. To reduce the burden of annotation, we study the problem of achieving 3D object detection solely based on 2D annotations. Thanks to advanced 3D reconstruction techniques, it is now feasible to reconstruct the overall static 3D scene. However, extracting precise object-level annotations from the entire scene and generalizing these limited annotations to the entire scene remain challenges. In this paper, we introduce a novel paradigm called BA²-Det, encompassing pseudo label generation and multi-stage generalization. We devise the DoubleClustering algorithm to obtain object clusters from reconstructed scene-level points, and further enhance the model’s detection capabilities by developing three stages of generalization: progressing from complete to partial, static to dynamic, and close to distant. Experiments conducted on the large-scale Waymo Open Dataset show that the performance of BA²-Det is on par with the fully-supervised methods using 10% annotations. Additionally, using large raw videos for pretraining, BA²-Det can achieve a 20% relative improvement on the KITTI dataset. The method also has great potential for detecting open-set 3D objects in complex scenes. Project page: <https://ba2det.site>.

1. Introduction

3D object detection has gained increasing attention from researchers and has become a fundamental task in real-

world perception. Thanks to the efforts of researchers, fully supervised 3D object detection is practical in both traffic scenes (Shi et al., 2020; Yin et al., 2021; Fan et al., 2023) and indoor scenes (Qi et al., 2019; Liu et al., 2021). In recent years, the cheap cost of camera sensors has fostered the emergence of image-based 3D object detection as a rapidly developing field of research, including monocular and multi-camera settings. In terms of performance, camera-only 3D object detectors (Wang et al., 2023) are also gradually catching up with LiDAR-based methods.

However, due to the requirement of extensive and costly manual annotations, the further development of fully supervised 3D object detection methods is potentially limited. To overcome this limitation, some previous works have explored weak supervision algorithms (Zakharov et al., 2020; Peng et al., 2022c) with additional LiDAR data to unlock the potential of unlabeled images. However, the reliance on LiDAR sensors limits the practicality of these methods in more general scenarios. With the advancement of 2D foundation models (Kirillov et al., 2023), 2D annotation is no longer a bottleneck. In this paper, we aim to investigate the feasibility of achieving 3D object detection solely based on 2D annotations, an unexplored problem.

The core challenge for this problem lies in deriving 3D information from 2D images. Drawing inspiration from 3D reconstruction techniques (Schoenberger & Frahm, 2016), we can obtain the overall static 3D scene structure. Therefore, the core challenge has shifted to *extracting object-level pseudo-labels from the global scene*, and *generalizing limited object pseudo-labels to more objects*.

To address this challenge, we introduce a novel paradigm called BA²-Det, consisting of Pseudo Label Generation and Multi-Stage Generalization. The Pseudo Label Generation phase generates object-level 3D bounding boxes based on the reconstructed 3D scene and 2D bounding boxes in each frame. We have devised a two-step clustering algorithm called *DoubleClustering*, consisting of intra-frame Local Point Clustering (LPC) and inter-frame Global Point Clustering (GPC). This algorithm ensures more complete and clean object clusters, from which we can easily obtain initial object pseudo-labels. However, these initial object pseudo-labels are only accurate for static and fully reconstructed objects. This is because moving objects cannot be recon-

¹CRIPAC, Institute of Automation, Chinese Academy of Sciences (CASIA) ²School of Artificial Intelligence, University of Chinese Academy of Sciences (UCAS) ³Centre for Artificial Intelligence and Robotics, HKISL-CAS. Correspondence to: Jiawei He <hejiawei2019@ac.cn>, Yuqi Wang <wangyuqi2020@ac.cn>, Yuntao Chen <chenyuntao08@gmail.com>, Zhaoxiang Zhang <zhaoxiang.zhang@ia.ac.cn>.

structured in scene-level 3D reconstruction, and some object clusters may be incomplete due to occlusion or far distance. To tackle this issue, our Multi-Stage Generalization leverages the generalization capability of neural network models. The first stage of generalization is from complete objects to partial ones. We learn the complete 3D bounding box of partial objects from other non-occluded 3D boxes using a PointNet-like neural network. The second stage of generalization is from static to dynamic. We develop a monocular 3D object detector that operates on single-frame images. This detector is capable of learning movement-agnostic 3D representations from monocular images, as there is no visual distinction between moving and stationary objects in an image. Additionally, we have devised a new label assignment strategy, orientation loss, and an iterative self-retraining strategy for efficient training of the detector using pseudo-labels. Finally, we also employ temporal aggregation, inspired by (He et al., 2023), to enhance close-to-distant generalization. With the help of these generalizations, our method can effectively adapt to full-scene 3D object detection. In summary, our main contributions are as follows:

- We propose a novel paradigm for weakly supervised monocular 3D object detection using only 2D labels. Leveraging 3D reconstruction and the generalization capabilities of neural networks, we present a practical solution to this problem for the first time.
- Our proposed method, named BA²-Det, addresses three fundamental technical challenges in learning the 3D object detector. We have developed three stages of generalizations: from complete to partial, from static to dynamic, and from close to distant.
- We conducted experiments on various datasets, including the KITTI dataset and the large-scale Waymo Open Dataset (WOD), demonstrating the effectiveness of our method for generating high-quality 3D labels and leveraging large-scale data for pretraining. The performance of BA²-Det is comparable to the fully-supervised BA-Det trained with only 10% of the videos, and even outperforms some leading fully-supervised methods. As a pretraining approach, BA²-Det can achieve a relative improvement of 20% on the KITTI dataset.
- We further investigate the potential impact of our method, including the detection of open-set 3D objects in complex scenes and the downstream application of 3D object tracking.

2. Related Work

2.1. Fully Supervised Monocular 3D Object Detection

Monocular 3D object detection (Chen et al., 2016; Brazil & Liu, 2019; Wang et al., 2019; Zhang et al., 2021) has been explored for several years. The existing monocular 3D object detection methods can be divided into three categories: regressing 3D objects from the image directly, regressing on the depth map or lifted 3D space, and regressing based on geometric constraints. CenterNet (Zhou et al., 2019) and FCOS3D (Wang et al., 2021c) are the representing works to estimate the 3D objects with a 3D regression branch based on the 2D object detectors. PL (Wang et al., 2019) and PL++ (You et al., 2020) use the off-the-shelf dense depth estimator to project the scene in 3D space and detect objects from pseudo-LiDAR. D4LCN (Ding et al., 2020) and PatchNet (Ma et al., 2020) use the image-aligned depth map to extract features. E2E-PL (Qian et al., 2020) and CaDDN (Reading et al., 2021) jointly learn the depth estimator and 3D object detector in an end-to-end manner. With the geometric constraints, the 3D object depth can be estimated by solving Perspective-n-Point (PnP) problem. MonoFlex (Zhang et al., 2021) solves PnP from the vertical lines of 3D bounding boxes. DCD (Li et al., 2022b) uses arbitrary point pairs to construct dense constraints. Recently, there has been a surge in the development of temporal 3D object detection from monocular images. DfM (Wang et al., 2022a) and BA-Det (He et al., 2023) aggregate temporal information at the scene level and in an object-centric manner, inspired by two-view and multi-view geometry theory.

2.2. Detecting 3D Objects without 3D Labels

Since the 3D object detection task made great progress in the past few years, many researchers have begun to explore using fewer 3D labels or even without 3D labels to train a 3D object detector. For LiDAR-based 3D object segmentation, clustering-based methods (Triebel et al., 2010; Campello et al., 2013; Nunes et al., 2022) are the mainstream methods. LSMOL (Wang et al., 2022b) and Najibi et al. (2022) combine image and LiDAR to segment 2D and 3D objects. However, only class-agnostic segmentation can be achieved in these methods. MODEST (You et al., 2022) is an unsupervised 3D mobile object detection method to predict 3D bounding box. Its key idea is that mobile objects are ephemeral members of a scene. For image-based 3D object detection, SDFLabel (Zakharov et al., 2020) is a pioneer work that can auto-label the 3D bounding boxes from a pre-trained 2D detector and the corresponding LiDAR data by recovering the object shape with signed distance fields (SDF). WeakM3D (Peng et al., 2022c) is also a weakly supervised method and needs additional LiDAR data. Yang et al. (2022) first explore the image-only weakly supervision without LiDAR. However, box size and orientation

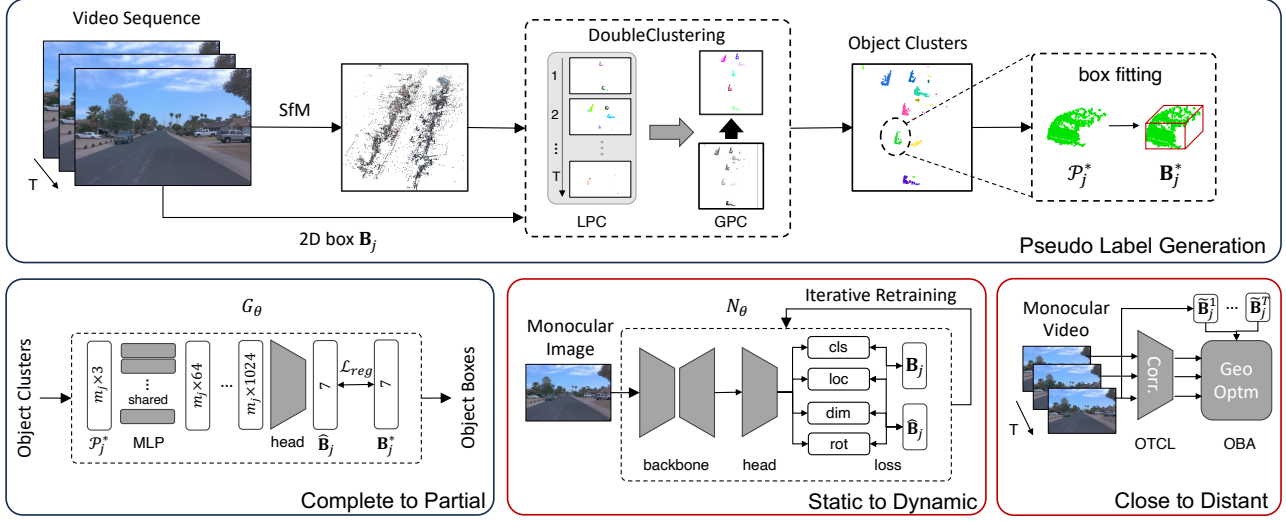


Figure 1: **Pipeline of BA²-Det.** Top: reconstruction-based pseudo label generation process. We cluster the object point clouds from the reconstructed scene and fit the tight bounding box as the pseudo label. Bottom: Three stages of network generalization. The neural networks inside the **red rounded rectangles** are also for the inference.

cannot be estimated in this method and can only be learned by ground truth in the semi-supervised setting. Unlike the above works, our BA²-Det *only uses images* without LiDAR as an auxiliary modality and can estimate 3D *bounding boxes* including center position, box size, and orientation.

Besides, there are some weakly supervised methods (Yang et al., 2021; Li et al., 2022a) designed for the 6DoF pose estimation task. However, these two tasks encounter distinct challenges. In 6DoF pose estimation, the models learn the rotation and translation of specific objects on the table or near the camera. The primary challenge in 3D object detection is accurately estimating the depth and pose of objects in distant and heavily occluded scenes. So there are significant differences in methodology and experimental details between 6DoF pose estimation and 3D object detection. Moreover, in our setting, we do not require additional 3D models (class-aware CAD models) as prior knowledge, which is the common practice in 6DoF pose estimation.

3. Methodology

Problem setup. In this paper, we present the task of weakly supervised monocular 3D object detection with only 2D labels. Our method is designed not to require detailed 2D object masks for supervision; only 2D bounding boxes are sufficient. The object predictions are represented as 7-dimensional 3D bounding boxes, i.e., object center location (c_x, c_y, c_z) in the camera frame, 3D box size (w, h, l), and yaw rotation r_y . The main difference between previous studies and ours is that our detector does not require training with 3D ground truth or the use of LiDAR data as an auxiliary modality. Our BA²-Det also does not rely on manually

crafted CAD models and pretrained depth models.

Algorithm overview. We introduce our framework BA²-Det briefly and explain module designs. As shown in Fig. 1, BA²-Det includes two main parts, high-quality pseudo label generation and multi-stage generalization from the pseudo labels. In **pseudo label generation** phase (Sec. 3.1), we first utilize scene-level reconstruction from the moving camera to obtain the global point clouds. To extract 3D object clusters from scene reconstruction, we design a *DoubleClustering* algorithm. The object clusters are further fitted with cuboids to form 3D bounding boxes. During the subsequent **multi-stage generalization** phase (Sec. 3.2), (1) To generalize *from complete to partial*, we develop a neural network to learn 3D object bounding boxes for partial objects from well-reconstructed objects; (2) To generalize *from static to dynamic*, we train a 3D object detector with carefully designed learning strategies and iterative refinement; (3) To generalize *from close to distant*, we follow learn temporal object detector with geometric feature aggregation.

3.1. Pseudo Label Generation from Scene-level Reconstruction

Using the Structure-from-Motion (SfM) technique, it is possible to reconstruct a 3D scene from ego-motion. Then from the reconstructed scene, with the help of 2D bounding boxes in each frame, the 3D object cluster can be obtained by clustering the foreground points from the reconstructed scene. So, in this section, we introduce an algorithm called *DoubleClustering* (Alg. 1) for extracting 3D object clusters from the 3D reconstructed scene. Then we optimize and

Algorithm 1 Generating object clusters (DoubleClustering)

Input: video clip \mathcal{V} , camera intrinsic $\{\mathbf{K}\}$, camera pose $\{\mathbf{T}_t\}$, 2D bounding box $\{\mathbf{B}_j^t\}_{j=1}^{n_d}$
Output: 3D object cluster $\{\mathcal{P}_j^*\}_{j=1}^{n_d}$

- 1: $\{\mathbf{P}_i^*\}_{i=1}^n \leftarrow \text{SfM}(\mathcal{V}, \{\mathbf{K}\}, \{\mathbf{T}_t\})$;
- 2: $\mathcal{P} \leftarrow \emptyset$;
- 3: **for** $j \in [1, n_d]$ **do** \triangleright LPC for each object in each frame
- 4: **for** $t \in [1, T]$ **do**
- 5: $\mathcal{P}_j^t \leftarrow \text{LPC}(\{\mathbf{P}_i^*\}, \mathbf{B}_j^t)$;
- 6: $\mathcal{P} \leftarrow \mathcal{P} \cup \mathcal{P}_j^t$;
- 7: $\{\mathcal{P}_{j'}\}_{j'=1}^{n_d'} \leftarrow \text{GPC}(\mathcal{P})$; \triangleright GPC from \mathcal{P} to generate n_d' clusters
- 8: $\{\mathcal{P}_j^*\}_{j=1}^{n_d} \leftarrow \text{Match}(\{\mathcal{P}_{j'}\}, \{\mathbf{B}_j^t\})$; \triangleright Match objects to the point clusters
- 9: **return** $\{\mathcal{P}_j^*\}_{j=1}^{n_d}$

generate tight 3D bounding boxes for each object cluster as an initial pseudo label.

Scene Reconstruction. Firstly, let's revisit scene reconstruction with SfM. We denote the video sequence as $\mathcal{V} = \{\mathbf{I}_t | t = 1, 2, \dots, T\}$, keypoints in image \mathbf{I}_t as $\mathbf{p}_t^i = [u_i, v_i]^\top$, ($i = 1, 2, \dots, n$) and local feature on each keypoint as $\mathcal{F}_t = \{\mathbf{f}_t^i\}$. In this paper, we use the keypoint extractor and local feature-matching network SuperPoint (DeTone et al., 2018) and SuperGlue (Sarlin et al., 2020). Given intrinsic parameter \mathbf{K} and the extrinsic parameter $\mathbf{T}_t = [\mathbf{R}_t | \mathbf{t}_t]$ of the camera in time t , 3D keypoint \mathbf{P}_i in the global frame can be optimized by solving bundle adjustment (BA) with projection error computed on the corresponding keypoints between any two images as

$$\{\mathbf{P}_i^*\}_{i=1}^n = \arg \min_{\{\mathbf{P}_i\}_{i=1}^n} \frac{1}{2} \sum_{i=1}^n \sum_{t=1}^T \|\mathbf{p}_t^i - \Pi(\mathbf{T}_t, \mathbf{P}_i, \mathbf{K})\|^2, \quad (1)$$

where $\Pi(\cdot)$ is the function projecting the 3D points in the world frame to the image. Besides, \mathbf{K} and \mathbf{T}_t can be also optimized in BA process. Please note that when the ego moves slowly, the disparity between two frames is small and the observation noise can affect reconstruction. Therefore, when the camera moves slowly, we disregard the video sequence and do not reconstruct the scene. The speed threshold is defined as ω .

Object point cloud clustering. After the scene reconstruction, we introduce a two-step object clustering algorithm, called DoubleClustering, to separate and cluster the object point clouds in the reconstructed scene. Firstly, in each frame, we choose the 3D points that can be projected in the 2D bounding boxes, and perform the Local Point Clustering (LPC) to choose the largest cluster for each object \mathbf{B}_j^t :

$$\mathcal{P}_j^t = \{\mathbf{P}_i\}_{i=1}^m = \text{LPC}(\{\mathbf{P}_i^* | \Pi(\mathbf{T}_t, \mathbf{P}_i^*, \mathbf{K}) \in \mathbf{b}_j^t\}), \quad (2)$$

where we denote \mathbf{b}_j^t as the image region in the 2D box \mathbf{B}_j^t . The cluster algorithm is based on Connected Component (CC) algorithm, and the distance threshold in CC algorithm is δ_1 .

Secondly, we gather the clusters from each frame, and conduct global clustering in the whole scene. The clustering algorithm is also based on CC with distance threshold δ_2 , called Global Point Clustering (GPC):

$$\{\mathcal{P}_{j'}\}_{j'=1}^{n_d'} = \text{GPC}(\bigcup_{t,j} \mathcal{P}_j^t), \quad (3)$$

where n_d' is the total object clusters. We ignore clusters with point numbers lower than threshold θ , as they may represent noise points. Finally, we choose the object cluster with the highest number of projected points in it as the corresponding cluster \mathcal{P}_j^* for the 2D bounding box \mathbf{B}_j^t .

3D bounding box fitting. We now obtain object clusters and then we need to generate the initial 3D pseudo box from the object points in each cluster. Given the object cluster \mathcal{P}_j^* , we fit a tight 3D bounding box according to the object points. These tight boxes serve as the initial 3D labels. Utilizing the assumption that the reconstructed points are mainly located on the object's surface and taking inspiration from Zhang et al. (2017), we optimize the orientation r_y by minimizing the total distance between the points and their closest edge. Subsequently, we adjust the width and length of the bird's-eye view bounding box to achieve minimal area:

$$r_y^*, \mathbf{B}_{bev}^* = \arg \min_{r_y \in [0, \pi], \mathbf{B}_{bev} \in \mathbb{R}^2} \sum_{i=1}^m \min_{l \in [1, 4]} d(\mathbf{P}_i, \mathbf{R}(r_y) \mathbf{B}_{bev}^l), \quad (4)$$

where \mathbf{P}_i is the 3D points in the object cluster, and $\mathbf{R}(r_y) \mathbf{B}_{bev}^l$ is the edge of rotated bounding box in Bird's Eye View (BEV) with angle r_y , we use l_2 distance as distance function $d(\cdot)$. We calculate the box's height using points along the z-axis. We calculate the box height by measuring the distance between the highest and lowest points of the point cloud along the z-axis, and finally generate the 3D box \mathbf{B}_j^* for object j .

3.2. Multi-Stage Generalization

Some objects may be occluded or influenced by outlier points. These partial objects have not been reconstructed well, resulting in inaccurate labels, especially for size and orientation estimation. So we design the first-stage complete-to-partial generalization. In the traditional SfM system, reconstructing points on static objects is easy, but it is challenging to reconstruct moving objects due to their different movement from ego-motion and being filtered by epipolar geometry constraints. Only *static* objects are in

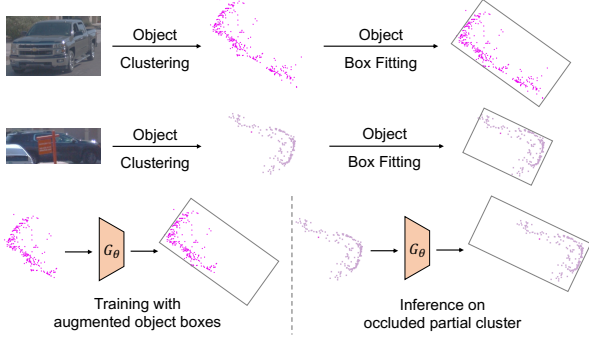


Figure 2: **Illustrations of fitted bounding boxes and generalized boxes.** Some occluded objects are badly reconstructed, leading to inaccurate pseudo-labels. G_θ can generalize from augmented complete objects to partial objects.

initial pseudo labels. So we propose the second-stage static-to-dynamic generalization. Besides, distant objects have fragile visual features. So we propose the third-stage close-to-distant temporal generalization.

Generalization from complete to partial objects. The first stage of generalization is to train a model to predict a full 3D bounding box from occluded/partial object point clouds. Therefore, we design a neural network G_θ to learn and refine the initial 3D bounding box from well-reconstructed complete objects. In general, we expect to first find the well-reconstructed/complete objects as training data, i.e., the objects whose 3D bounding box can be correctly fitted from the object point clouds. Then learning from these objects, the network can predict full 3D boxes for all object clusters. Fig 2 shows how does G_θ work.

This network takes the object cluster $\mathcal{P}_j^* \in \mathbb{R}^{m_j \times 3}$ as input and normalizes the coordinates of 3D points using the center of the initial 3D pseudo box \mathbf{B}_j^* . It consists of a PointNet backbone and a head to predict 7DoF 3D bounding box $\hat{\mathbf{B}}_j = [c_x, c_y, c_z, w, h, l, r_y]$. We use the smooth L1 bounding box localization loss \mathcal{L}_{reg} . Note that we only consider the length between $[\sigma_0, \sigma_1]$ as the well-reconstructed object and take these 3D pseudo boxes to supervise G_θ . To simulate the occlusion-induced partial object points, we perform data augmentation by randomly cutting off regions from the well-reconstructed object cluster. More details in training G_θ are in Sec. A.3.5 in the appendix.

Generalization from static to moving objects. We still need to address the issue that pseudo labels mainly come from static objects. We observe that in a single monocular image, static and moving objects have similar appearances. Therefore, the network can generalize the 3D object predictions learning from static labels to other moving objects. We denote the monocular 3D object detector as N_θ . The network architecture is based on CenterNet (Zhou et al., 2019;

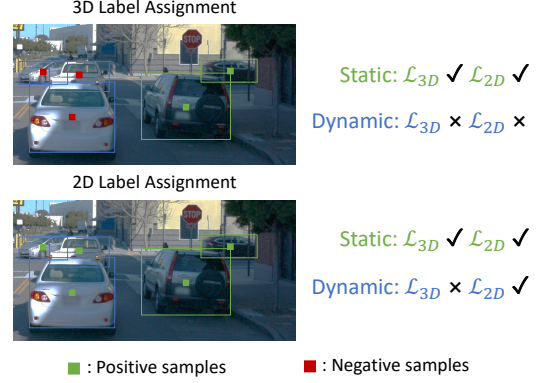


Figure 3: **Comparison between 2D and 3D label assignment.** For 3D label assignment used in fully supervised setting, moving objects are negative samples. However, our 2D label assignment keeps them as positive samples.

Zhang et al., 2021). In our weakly supervised setting, many objects have 2D labels \mathbf{B}_j , but there are no corresponding 3D pseudo labels $\hat{\mathbf{B}}_j$ due to their movement. Besides, the pseudo labels $\hat{\mathbf{B}}_j$ may have inaccurate orientation. So, different from a fully supervised object detector, we design a new label assignment strategy and orientation loss.

Regarding the issue of unlabeled moving objects, training the network with traditional 3D label assignment will lead to many false negatives. We assign labels using 2D ground truth (GT) labels and disregard their 3D losses if there are no 3D pseudo labels as

$$\mathcal{L}_{3D}(u, v) = \begin{cases} 0, & \text{if } (u, v) \notin \mathcal{C}, \\ \mathcal{L}_{loc} + \mathcal{L}_{dim} + \mathcal{L}_r, & \text{else,} \end{cases} \quad (5)$$

which (u, v) is the pixel on the image, and $\mathcal{C} = \{(c_u, c_v) | [(c_u, c_v) \text{ is center of } \mathbf{B}_j] \wedge [\hat{\mathbf{B}}_j \neq \emptyset]\}$. As shown in Fig. 3, the proposed 2D assignment ensures that the unlabeled objects are not considered negative samples.

Another difficulty for weak supervision is to distinguish whether the object is facing forward or backward. The orientation of the 3D pseudo label may have a deviation of 180° from the real heading. We modify the original Multi-Bin orientation loss (Mousavian et al., 2017) to alleviate this problem. The new orientation loss is the minimum in original loss and 180° -reversed one:

$$\mathcal{L}_r = \min(\mathcal{L}_M(\hat{r}_y, r_y), \mathcal{L}_M(\pi + \hat{r}_y, r_y)), \quad (6)$$

where \mathcal{L}_M is MultiBin Loss, \hat{r}_y is yaw prediction, r_y is pseudo ground truth.

To further refine the generalized object boxes, we iteratively retrain the detector with predictions as the updated pseudo labels. We adopt a retraining strategy of using 3D pseudo labels for initial training and updating labels with predictions

Method	Tem.	3D Sup.	3D AP ₅	3D APH ₅	3D AP ₅₀	3D APH ₅₀	LET AP _{L50}	LET AP ₅₀	LET APH ₅₀
PatchNet (Ma et al., 2020)		100% [†]	-	-	2.92	2.74	-	-	-
M3D-RPN (Brazil & Liu, 2019)		100% [†]	-	-	3.79	3.63	-	-	-
PCT (Wang et al., 2021a)		100% [†]	-	-	4.20	4.15	-	-	-
MonoJSG (Lian et al., 2022)		100% [†]	-	-	5.65	5.47	-	-	-
BA²-Det (Ours)		0% [†]	55.24	40.87	6.24	5.37	16.61	27.94	21.32
MonoFlex (Zhang et al., 2021)		100%	70.33	69.41	34.70	34.43	50.63	67.30	66.50
BA-Det (He et al., 2023)	✓	100%	72.96	71.78	40.93	40.51	54.45	68.32	67.36
MonoFlex (Zhang et al., 2021)		10%	53.68	52.30	15.44	15.22	28.21	44.21	43.23
BA-Det (He et al., 2023)	✓	10%	57.29	55.27	19.70	19.27	32.53	46.91	45.52
BA²-Det (Ours)	✓	10%	65.24	62.95	25.17	24.65	42.55	58.77	57.14
SfM+BA-Det (Baseline)	✓	0%	27.84	8.80	2.89	0.75	7.34	10.75	3.31
BA²-Det (Ours)	✓	0%	60.01	44.81	10.39	8.98	22.24	32.60	23.86

Table 1: **The main results on WOD *val* set.** ‘3D Sup.’ means the ratio of video sequences with 3D labels. ‘Tem.’ means using a temporal object detector. †: trained with 1/3 frames.

Method	Extra Data	Easy	Mod.	Hard
PatchNet (Ma et al., 2020)	Raw+depth	15.68	11.12	10.17
PCT (Wang et al., 2021a)	-	21.00	13.37	11.31
GUPNet (Lu et al., 2021)	-	22.26	15.02	13.12
MonoDTR (Huang et al., 2022)	-	21.99	15.39	12.73
DCD (Li et al., 2022b)	CAD models	23.81	15.90	13.21
MonoJSG (Lian et al., 2022)	-	24.69	16.14	13.64
DID-M3D (Peng et al., 2022b)	-	24.40	16.29	13.75
LPCG (Peng et al., 2022a)	Raw+LiDAR	25.56	17.80	15.38
CMKD (Hong et al., 2022)	Raw+LiDAR	28.55	18.69	16.77
MonoFlex (Zhang et al., 2021)	-	19.94	13.89	12.07
BA²-Det+MonoFlex (Ours)	Raw	23.45	16.30	13.50
<i>Improvement</i>		<i>+3.51</i>	<i>+2.41</i>	<i>+1.43</i>

Table 2: **The results on *test* set of KITTI detection benchmark.** ‘Raw’ means using images in KITTI Raw set. ‘Mod.’ means the moderate level of difficulty.

from the last iteration

$$\begin{cases} \mathcal{D}^{(0)}(X, Y) = N_{\theta}^{(0)}(\tilde{\mathcal{D}}(X, Y)), \\ \mathcal{D}^{(l)}(X, Y) = N_{\theta}^{(l)}(\mathcal{D}^{(l-1)}(X, Y)), \end{cases} \quad (7)$$

where $\tilde{\mathcal{D}}(X, Y)$ is the dataset with generated pseudo labels, $\mathcal{D}^{(l)}(X, Y)$ is the dataset with predicted labels, (l) means the l -th self-training iteration. Note that we do not keep the last network parameters for each self-retraining iteration and train the network N_{θ} for the same κ epochs.

Generalization from close to distant objects. A natural challenge for the monocular 3D object detector is that distant objects have fewer pixels, making it difficult to estimate their 3D position, especially depth estimation. Inspired by BA-Det (He et al., 2023), we utilize geometric temporal aggregation to generalize the close objects to distant objects. Specifically, we learn the object-centric feature correspondence for an object with the object-centric temporal correspondence learning (OTCL) module and solve object-centric bundle adjustment (OBA) between the tracked object prediction $\{\tilde{\mathbf{B}}_j^1, \tilde{\mathbf{B}}_j^2, \dots, \tilde{\mathbf{B}}_j^T\}$ from N_{θ} during inference.

4. Experiments

4.1. Datasets and metrics

Waymo open dataset (WOD). To verify our proposed BA²-Det, we conduct our ablation studies and comparison experiments with other methods on the large-scale autonomous driving dataset, Waymo Open Dataset (WOD) (Sun et al., 2020). WOD is the mainstream 3D object detection benchmark, containing 1150 video sequences, 798 for training, 202 for validation, and 150 for testing. Only objects within 75m that can be scanned by LiDAR have 3D labels. To keep the same experiment settings as other methods, we mainly report the results on WOD v1.2. The evaluation metrics for camera-based 3D object detection are 3D AP and LET-3D AP (Hung et al., 2022). 3D AP is a common metric for both camera and LiDAR-based 3D object detection. LET-3D AP is specifically designed for camera-only 3D object detection. Because the camera-based 3D object detector has a natural weakness in depth estimation, LET-3D AP is much looser for longitudinal localization and uses Longitudinal Error Tolerant IoU (LET-IoU) instead of the original IoU as the criterion. Following the existing camera-based 3D object detection methods, we mainly report the results of the VEHICLE class on the FRONT camera. For 3D AP and 3D APH, we choose a loose IoU threshold of 0.05 and a common one of 0.5, called AP₅ and AP₅₀. For LET-3D metrics, we report the results under the official IoU threshold of 0.5.

KITTI dataset. KITTI object detection benchmark consists of 7481 images for training and 7518 images for testing. Unlike WOD, it is not organized as long video sequences. The main evaluation metric is 3D AP on three difficulty levels, easy, moderate, and hard. Besides the object detection benchmark, KITTI also provides the raw dataset without 3D object labels. We train BA²-Det on KITTI raw dataset.

	3D Ass.	2D Ass.	G_θ	Ori.	Iter.	OBA	3D AP ₅	3D APH ₅	LET APL ₅₀	LET AP ₅₀
(a)	✓						20.97	6.70	4.27	7.28
(b)		✓					28.40	11.34	5.02	8.62
(c)		✓	✓				33.75	11.94	9.63	16.80
(d)		✓	✓	✓			41.17	28.73	12.23	21.41
(e)		✓	✓	✓	✓		56.33	42.05	17.87	29.62
(f)		✓	✓	✓	✓	✓	60.01	44.81	22.24	32.60

Table 3: **The ablation study on BA²-Det.** The gray cells mean complete to partial , static to dynamic , close to distant generalization stages respectively.

4.2. Implementation Details

For 3D object detector, we use a DLA-34 (Yu et al., 2018) as the backbone without an FPN neck, and the head is with 2 layers of 3×3 convolutions and MLP. The resolution of the input images is 1920×1280 . If the input size is smaller than it, we will use zero padding to complete the image. The scene reconstruction is based on hloc (Sarlin et al., 2019) framework. The speed filtering threshold ω is 1m/s. The distance threshold δ_1 and δ_2 in DoubleClustering are 0.5 and 0.7. We keep the object cluster for more than $\theta = 100$ points. The size threshold $\sigma_0 = 3m$ and $\sigma_1 = 10m$. Our implementation is based on the PyTorch (Paszke et al., 2019) framework. We train our model on 8 NVIDIA RTX 4090 GPUs. Adam (Kingma & Ba, 2014) optimizer is applied with $\beta_1 = 0.9$ and $\beta_2 = 0.999$. The learning rate is 8×10^{-5} and weight decay is 10^{-5} . We train 1 epoch for network G_θ and $\kappa = 12$ epochs for the 3D object detector N_θ . The loss weights are the same as BA-Det. The self-retrain iteration number for N_θ is 2. As shown in Table 7, we choose labels in the wider depth range [0.5m, 200m] for initial training and regular range [0.5m, 75m] for iterative self-retraining.

4.3. Main Results

As shown in Table 1, we show the main results compared with fully-supervised BA-Det, a simple solution combining SfM and BA-Det, and some other fully supervised methods. Especially, to make a clear understanding of our results, we also compare the results of BA-Det trained with fewer data. We find that with a loose IoU threshold (0.05), our BA²-Det can outperform fully-supervised BA-Det with 10% data by 2.7 AP and is close to the 100% data (with a ~ 12 AP gap). As for the 0.5 IoU threshold, we can beat some other fully-supervised methods, such as PCT and MonoJSG. Compared with our baseline method, using SfM (Schonberger & Frahm, 2016) and clustering to fit 3D labels and learning a BA-Det, our BA²-Det have huge gains on all metrics. Besides, we also conduct experiments on the semi-supervised setting with the same 10% GT as BA-Det and MonoFlex and show better performance.

We also conduct experiments on KITTI (Geiger et al., 2012)

Iter.	3D AP ₅	3D APH ₅	LET APL ₅₀	LET AP ₅₀
0	41.17	28.73	12.23	21.41
1	51.81	38.66	17.42	28.57
2	56.33	42.05	17.87	29.62
3	56.70	42.27	16.87	28.06
4	57.12	42.42	16.64	27.73

Table 4: **Discussion about self-retraining iterations.**

to compare with other SOTA methods. We report 3D object detection results on test set. Note that (1) there is no long video for 3D reconstruction on KITTI object detection dataset, and we have to generate 3D pseudo boxes on KITTI raw dataset; (2) there are hardly any comparable methods available for 2D supervised 3D detection. So, we report the results taking BA²-Det as the pretraining approach. We pre-train BA²-Det on KITTI raw dataset without any labels (We use the 2D object detector Mask R-CNN trained on COCO) and finetune the monocular 3D object detector MonoFlex with 3D ground truth on KITTI detection training set. We only use a single frame during inference for a fair comparison. The results have been shown in Table 2. BA²-Det can have 2.4 AP gain (about 20% relative improvement) on the moderate level.

4.4. Ablation Study

We conduct the ablation study on WOD val set. Results are shown in Table 3. (a) ‘3D Ass.’ and (b) ‘2D Ass.’ mean we assign labels based on 3D or 2D (pseudo) labels (Fig. 3). 3D assignment will keep the recall and enhance the refinement of the 3D position during the iterative self-retraining stage. (c) G_θ learns a complete 3D box from the partially reconstructed object, that can obtain a 5.4 AP gain. (d) ‘Ori.’ is the orientation optimization, improving 16.8 APH by refining the orientation and box size. (e) Iterative self-retraining (Iter.) has the greatest gain of 15.2 AP. Comparing (e) and (f), with temporal OBA, 3D bounding boxes can generalize from near to far, which improves 3.7 AP. For more ablation studies, please refer to the appendix.

	Ratio	$\delta < 1.25 \uparrow$	$\delta < 1.25^2 \uparrow$	$\delta < 1.25^3 \uparrow$	Abs Rel \downarrow	Sq Rel \downarrow	RMSE \downarrow	RMSE log \downarrow
w/o p.l.	52.2%	0.991	0.994	0.995	0.055	0.324	2.773	0.100
w/ p.l.	47.8%	0.995	0.996	0.997	0.049	0.117	1.726	0.077
All	100%	0.992	0.995	0.996	0.053	0.266	2.524	0.094

Table 5: **Satic-to-dynamic generalization ability of 3D localization on WOD training set.** ‘w/o p.l.’: objects without pseudo label, ‘w/ p.l.’: objects with pseudo label.

Strategy	3D AP ₅	3D APH ₅	LET APL ₅₀	LET AP ₅₀
w/o iter.	41.17	28.73	12.23	21.41
Eq. 8	39.71 \downarrow 1.5	29.79 \uparrow 1.0	12.75 \uparrow 0.5	21.08 \downarrow 0.3
Eq. 7	51.81 \uparrow 10.6	38.66 \uparrow 9.9	17.42 \uparrow 5.2	28.57 \uparrow 7.2

Table 6: **Ablation study on self-retraining strategy.**

Iter.	Depth (m)	3D AP ₅	3D APH ₅	LET APL ₅₀	LET AP ₅₀
0	[0.5, 75]	22.24	7.66	4.83	8.56
0	all, [0.5, 200]	33.75	11.94	9.63	16.80
1	[0.5, 75]	42.07	15.00	12.32	20.48
1	all, [0.5, 200]	40.60	14.49	12.18	20.05

Table 7: **Experiments for different depth thresholds.**

4.5. Discussions

Self-retraining iteration. We discuss the number of iterations required for the self-retraining stage. In Table 4, we conduct the experiments of a maximum of 4 iterations. The first iteration can bring the greatest benefit of 10.7 AP and the benefits are progressively decreased. After the second iteration, the performance is near the highest performance, which shows fast convergence of the self-retraining stage.

Retraining strategy. In the static to dynamic generalization stage, we propose the iterative retraining strategy (Eq. 7). Another feasible retraining strategy can be keeping the initial 3D pseudo labels and supplementing the high score predictions iteratively

$$\mathcal{D}^{(l)}(X, Y) = N_{\theta}^{(l)}(\tilde{\mathcal{D}}(X, Y) \cup \mathcal{D}^{(l-1)}(X, Y)), \quad (8)$$

In Table 6, we show the experiment results of retaining 1 iteration. The strategy in Eq. 7 is much better. The combination of pseudo-labels and predictions may introduce two inconsistent data distributions, causing poor results. The results in Table 3 and Table 4 also indicate the importance of the chosen self-retraining strategy.

Depth threshold settings. By utilizing reconstruction, we can generate labels for objects that are farther away, and thus the depth distribution is different from ground truth, shown in Fig. 4. According to experiments (Table 7), we find that when we initially train the object detector, we need these farther objects, and for iteratively self-retraining, we can only train with the same depth ranges as the ground

truth (0-75m).

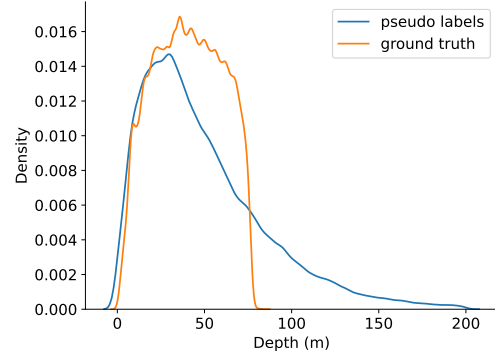


Figure 4: **Depth distributions of ground truth and pseudo labels.** BA²-Det can generate pseudo labels up to a maximum of 200m, whereas the ground truth labels range from 0m to 75m.

3D location results for static to dynamic generalization.

In Table 5, we validate the performance of generalizing 3D location for unlabeled objects. The metrics follow depth estimation but on the object level. We find that only 47.8% objects can be generated 3D pseudo labels directly. The others are mostly moving objects. The small gap between labeled and unlabeled objects in performance shows the static-to-dynamic generalization of the network N_{θ} .

Open-set 3D object detection, 3D tracking results, more ablation studies, discussions, qualitative results, limitations, and broader impacts. Please refer to the appendix. For video demos, please refer to <https://ba2det.site>.

5. Conclusion

In this paper, we propose BA²-Det, a novel paradigm for 2D supervised monocular 3D object detection. The key idea of BA²-Det is to generate 3D pseudo labels from scene-level global reconstruction and learn neural networks to generalize pseudo labels in multi-stage. Specifically, in pseudo label generation phase, objects are clustered by the proposed DoubleClustering algorithm and fitted into bounding boxes. In multi-stage generalization phase, we design three stages of generalization: progressing from complete to partial, static to dynamic, and near to far. Experiments on the large-scale Waymo Open Dataset show that the performance of

BA²-Det is on par with the fully-supervised BA-Det trained with 10% videos and even outperforms some pioneering fully-supervised methods. As a pretraining method, BA²-Det can bring 20% relative improvement on KITTI dataset. We also show the potential of BA²-Det for detecting open-set 3D objects in complex scenes.

References

- Brazil, G. and Liu, X. M3d-rpn: Monocular 3d region proposal network for object detection. In *ICCV*, 2019.
- Campello, R. J., Moulavi, D., and Sander, J. Density-based clustering based on hierarchical density estimates. In *KDD*, 2013.
- Chen, X., Kundu, K., Zhang, Z., Ma, H., Fidler, S., and Urtasun, R. Monocular 3d object detection for autonomous driving. In *CVPR*, 2016.
- DeTone, D., Malisiewicz, T., and Rabinovich, A. Superpoint: Self-supervised interest point detection and description. In *CVPR Workshops*, 2018.
- Ding, M., Huo, Y., Yi, H., Wang, Z., Shi, J., Lu, Z., and Luo, P. Learning depth-guided convolutions for monocular 3d object detection. In *CVPR*, 2020.
- Fan, L., Yang, Y., Wang, F., Wang, N., and Zhang, Z. Super sparse 3d object detection. *arXiv preprint arXiv:2301.02562*, 2023.
- Fischer, T., Yang, Y.-H., Kumar, S., Sun, M., and Yu, F. Cc-3dt: Panoramic 3d object tracking via cross-camera fusion. *arXiv preprint arXiv:2212.01247*, 2022.
- Geiger, A., Lenz, P., and Urtasun, R. Are we ready for autonomous driving? the kitti vision benchmark suite. In *CVPR*, 2012.
- He, J., Chen, Y., Wang, N., and Zhang, Z. 3d video object detection with learnable object-centric global optimization. In *CVPR*, 2023.
- Hong, Y., Dai, H., and Ding, Y. Cross-modality knowledge distillation network for monocular 3d object detection. In *ECCV*, 2022.
- Hu, H.-N., Yang, Y.-H., Fischer, T., Darrell, T., Yu, F., and Sun, M. Monocular quasi-dense 3d object tracking. *IEEE Transactions on Pattern Analysis and Machine Intelligence*, 45(2):1992–2008, 2022.
- Huang, K.-C., Wu, T.-H., Su, H.-T., and Hsu, W. H. Monodtr: Monocular 3d object detection with depth-aware transformer. In *CVPR*, 2022.
- Hung, W.-C., Kretschmar, H., Casser, V., Hwang, J.-J., and Anguelov, D. Let-3d-ap: Longitudinal error tolerant 3d average precision for camera-only 3d detection. *arXiv preprint arXiv:2206.07705*, 2022.
- Kingma, D. P. and Ba, J. Adam: A method for stochastic optimization. *arXiv preprint arXiv:1412.6980*, 2014.
- Kirillov, A., Mintun, E., Ravi, N., Mao, H., Rolland, C., Gustafson, L., Xiao, T., Whitehead, S., Berg, A. C., Lo, W.-Y., et al. Segment anything. *arXiv preprint arXiv:2304.02643*, 2023.
- Li, F., Shugurov, I., Busam, B., Yang, S., and Ilic, S. Ws-ope: Weakly supervised 6-d object pose regression using relative multi-camera pose constraints. *IEEE Robotics and Automation Letters*, 7(2):3703–3710, 2022a.
- Li, Y., Chen, Y., He, J., and Zhang, Z. Densely constrained depth estimator for monocular 3d object detection. In *ECCV*, 2022b.
- Lian, Q., Li, P., and Chen, X. Monojsq: Joint semantic and geometric cost volume for monocular 3d object detection. In *CVPR*, 2022.
- Liu, Z., Zhang, Z., Cao, Y., Hu, H., and Tong, X. Group-free 3d object detection via transformers. In *ICCV*, 2021.
- Lu, Y., Ma, X., Yang, L., Zhang, T., Liu, Y., Chu, Q., Yan, J., and Ouyang, W. Geometry uncertainty projection network for monocular 3d object detection. In *ICCV*, 2021.
- Ma, X., Liu, S., Xia, Z., Zhang, H., Zeng, X., and Ouyang, W. Rethinking pseudo-lidar representation. In *ECCV*, 2020.
- Mousavian, A., Anguelov, D., Flynn, J., and Kosecka, J. 3d bounding box estimation using deep learning and geometry. In *CVPR*, 2017.
- Najibi, M., Ji, J., Zhou, Y., Qi, C. R., Yan, X., Ettinger, S., and Anguelov, D. Motion inspired unsupervised perception and prediction in autonomous driving. In *ECCV*, 2022.
- Nunes, L., Chen, X., Marcuzzi, R., Osep, A., Leal-Taixé, L., Stachniss, C., and Behley, J. Unsupervised class-agnostic instance segmentation of 3d lidar data for autonomous vehicles. *IEEE Robotics and Automation Letters*, 7(4):8713–8720, 2022.
- Paszke, A., Gross, S., Massa, F., Lerer, A., Bradbury, J., Chanan, G., Killeen, T., Lin, Z., Gimelshein, N., Antiga, L., et al. Pytorch: An imperative style, high-performance deep learning library. *NeurIPS*, 2019.

- Peng, L., Liu, F., Yu, Z., Yan, S., Deng, D., Yang, Z., Liu, H., and Cai, D. Lidar point cloud guided monocular 3d object detection. In *ECCV*, 2022a.
- Peng, L., Wu, X., Yang, Z., Liu, H., and Cai, D. Didm3d: Decoupling instance depth for monocular 3d object detection. In *ECCV*, 2022b.
- Peng, L., Yan, S., Wu, B., Yang, Z., He, X., and Cai, D. Weakm3d: Towards weakly supervised monocular 3d object detection. *arXiv preprint arXiv:2203.08332*, 2022c.
- Qi, C. R., Litany, O., He, K., and Guibas, L. J. Deep hough voting for 3d object detection in point clouds. In *ICCV*, 2019.
- Qian, R., Garg, D., Wang, Y., You, Y., Belongie, S., Hariharan, B., Campbell, M., Weinberger, K. Q., and Chao, W.-L. End-to-end pseudo-lidar for image-based 3d object detection. In *CVPR*, 2020.
- Reading, C., Harakeh, A., Chae, J., and Waslander, S. L. Categorical depth distribution network for monocular 3d object detection. In *CVPR*, 2021.
- Sarlin, P.-E., Cadena, C., Siegwart, R., and Dymczyk, M. From coarse to fine: Robust hierarchical localization at large scale. In *CVPR*, 2019.
- Sarlin, P.-E., DeTone, D., Malisiewicz, T., and Rabinovich, A. Superglue: Learning feature matching with graph neural networks. In *CVPR*, 2020.
- Schonberger, J. L. and Frahm, J.-M. Structure-from-motion revisited. In *CVPR*, 2016.
- Shi, S., Guo, C., Jiang, L., Wang, Z., Shi, J., Wang, X., and Li, H. Pv-rcnn: Point-voxel feature set abstraction for 3d object detection. In *CVPR*, 2020.
- Sun, P., Kretschmar, H., Dotiwalla, X., Chouard, A., Patnaik, V., Tsui, P., Guo, J., Zhou, Y., Chai, Y., Caine, B., et al. Scalability in perception for autonomous driving: Waymo open dataset. In *CVPR*, 2020.
- Triebel, R., Shin, J., and Siegwart, R. Segmentation and unsupervised part-based discovery of repetitive objects. In *RSS*, 2010.
- Wang, L., Zhang, L., Zhu, Y., Zhang, Z., He, T., Li, M., and Xue, X. Progressive coordinate transforms for monocular 3d object detection. *NeurIPS*, 2021a.
- Wang, Q., Chen, Y., Pang, Z., Wang, N., and Zhang, Z. Immortal tracker: Tracklet never dies. *arXiv preprint arXiv:2111.13672*, 2021b.
- Wang, S., Liu, Y., Wang, T., Li, Y., and Zhang, X. Exploring object-centric temporal modeling for efficient multi-view 3d object detection. In *ICCV*, 2023.
- Wang, T., Zhu, X., Pang, J., and Lin, D. Fcos3d: Fully convolutional one-stage monocular 3d object detection. In *ICCV*, 2021c.
- Wang, T., Pang, J., and Lin, D. Monocular 3d object detection with depth from motion. In *ECCV*, 2022a.
- Wang, Y., Chao, W.-L., Garg, D., Hariharan, B., Campbell, M., and Weinberger, K. Q. Pseudo-lidar from visual depth estimation: Bridging the gap in 3d object detection for autonomous driving. In *CVPR*, 2019.
- Wang, Y., Chen, Y., and ZHANG, Z.-X. 4d unsupervised object discovery. In *NeurIPS*, 2022b.
- Yang, J., Wang, T., Ge, Z., Mao, W., Li, X., and Zhang, X. Towards 3d object detection with 2d supervision. *arXiv preprint arXiv:2211.08287*, 2022.
- Yang, Z., Yu, X., and Yang, Y. Dsc-posenet: Learning 6dof object pose estimation via dual-scale consistency. In *CVPR*, 2021.
- Yin, T., Zhou, X., and Krahenbuhl, P. Center-based 3d object detection and tracking. In *CVPR*, 2021.
- You, Y., Wang, Y., Chao, W.-L., Garg, D., Pleiss, G., Hariharan, B., Campbell, M., and Weinberger, K. Q. Pseudo-lidar++: Accurate depth for 3d object detection in autonomous driving. In *ICLR*, 2020.
- You, Y., Luo, K., Phoo, C. P., Chao, W.-L., Sun, W., Hariharan, B., Campbell, M., and Weinberger, K. Q. Learning to detect mobile objects from lidar scans without labels. In *CVPR*, 2022.
- Yu, F., Wang, D., Shelhamer, E., and Darrell, T. Deep layer aggregation. In *CVPR*, 2018.
- Zakharov, S., Kehl, W., Bhargava, A., and Gaidon, A. Autolabeling 3d objects with differentiable rendering of sdf shape priors. In *CVPR*, 2020.
- Zhang, X., Xu, W., Dong, C., and Dolan, J. M. Efficient l-shape fitting for vehicle detection using laser scanners. In *IV*, 2017.
- Zhang, Y., Lu, J., and Zhou, J. Objects are different: Flexible monocular 3d object detection. In *CVPR*, 2021.
- Zhou, X., Wang, D., and Krähenbühl, P. Objects as points. *arXiv preprint arXiv:1904.07850*, 2019.

A. Additional Experiments

A.1. 3D Tracking Results

	Fully Sup.	MOTA ₅₀ ↑	Mismatch ₅₀ ↓	MOTA ₃₀ ↑	Mismatch ₃₀ ↓
QD-3DT (Hu et al., 2022)	✓	0.0308	0.00550	0.1867	0.01340
CC-3DT (Fischer et al., 2022)	✓	0.0480	0.00180	0.2032	0.00690
SfM+BA-Det+Immortal (Wang et al., 2021b)		0.0011	<0.00001	0.0652	0.00038
BA ² -Det (Ours)		0.0352	0.00002	0.1522	0.00008

Table 8: Comparisons with SOTA methods on WOD for 3D MOT.

In Table 8, we show additional 3D MOT results on WOD. We compare the proposed BA²-Det with other SOTA monocular 3D MOT methods on WOD. All results are reported in Vehicle LEVEL 2 difficulty. 50 and 30 in the metrics are for the IoU threshold of 0.5 and 0.3. Note that the SOTA methods are both fully supervised, learning with 3D ground truth. Our BA²-Det is a 2D supervised 3D multiple object tracking method. Even though, BA²-Det is also comparable to these fully supervised ones. Especially for MOTA₅₀ metric, we outperform QD-3DT (Hu et al., 2022). For Mismatch, we only have less than 1/100 identity switches compared with the SOTA methods. Compared with the baseline method, using SfM to generate pseudo labels, BA-Det as the 3D object detector, and ImmortalTracker to track 3D objects, our method BA²-Det improves the performance by a large margin.

A.2. Open-Set 3D Object Detection with SAM

In Fig. 5, we also show the ability to detect open-set 3D objects in complex scenes with SAM (Kirillov et al., 2023) instead of 2D ground truth. We click the objects to generate the 2D masks in SAM. Please refer to the detailed video demos from the project page.



Figure 5: **Open-set 3D object detection from a video sequence.** For the video demos for 3D box generation, please refer to our project page.

A.3. Additional Ablation Studies and Discussions

A.3.1. DETAILED RESULTS IN DIFFERENT DEPTH RANGES.

The detailed results in different depth ranges are shown in Table 9. Compared with the baseline, we have a more significant gain for the objects far off.

Weakly Supervised 3D Object Detection with Multi-Stage Generalization

Method	3D Sup.	3D AP ₅			3D APH ₅			LET APL ₅₀			LET AP ₅₀		
		0-30	30-50	50-∞	0-30	30-50	50-∞	0-30	30-50	50-∞	0-30	30-50	50-∞
BA-Det	100%	87.80	72.52	48.45	86.91	71.52	46.98	66.15	57.97	36.44	82.74	69.58	45.77
BA-Det	10%	73.25	54.00	34.50	71.38	52.22	32.53	38.31	35.57	22.40	56.98	47.28	31.11
SfM+BA-Det	0%	46.87	25.88	9.09	14.26	8.86	2.84	11.35	7.74	2.60	17.59	10.12	3.48
BA ² -Det (Ours)	0%	77.38	54.95	33.74	64.54	37.57	21.64	25.00	23.97	14.63	39.24	31.73	20.30

Table 9: The detailed results in different depth ranges (meters) on WOD val set.

A.3.2. ROBUSTNESS ACROSS VARIOUS LEVELS OF RECONSTRUCTION QUALITY.

Due to variations in reconstruction quality being primarily caused by differences in descriptors and matching algorithms, we simulate a scenario where there is a 25% decrease in the number of matched points due to failed matching. The results are presented in Table 10. The results show that our method is robust to the worse reconstruction quality.

	3D AP ₅	3D APH ₅	LET APL ₅₀	LET AP ₅₀
75% points	37.02	26.20	9.75	17.19
100% points	41.17	28.73	12.23	21.41

Table 10: Results with worse reconstruction. We simulate worse point matching case.

A.3.3. ROBUSTNESS ACROSS VARIOUS LEVELS OF 2D ANNOTATION QUALITY.

We discuss two kinds of worse 2D annotation qualities. The first is the influence of box numbers. We randomly drop 5% 2D bounding boxes and add 5% false positives. The second is for the 2D bounding box position. We add a maximum of 20% position error to the 4 corner points of the 2D bounding box. The results are shown in Table 11. Our method is relatively robust to the 2D box quality. Note that 2D object detection is a very stable and reliable technology. The 2D object detector is usually no worse than this simulation experiment. (For vehicles, >80 AP under 0.7 IoU threshold.)

	3D AP ₅	3D APH ₅	LET APL ₅₀	LET AP ₅₀
GT box	41.17	28.73	12.23	21.41
Add FP + FN	36.96	26.24	9.34	16.51
Inaccurate box position	31.34	21.88	8.45	14.81

Table 11: Results using worse 2D annotations.

A.3.4. NECESSITY OF LOCAL POINT CLUSTERING (LPC).

LPC has two main roles: (1) provide semantic labels (class and ID) for reconstructed 3D points; (2) remove background points in the 2D box (2D box is not tight enough for the object boundary). If only using GPC to remove background points, the background points in frame A may be close to the foreground points in frame B (because there are more points, points are near to each other globally), and thus the clustering is not easy. Besides, without LPC, there will be more points to be clustered in GPC, which takes more memory and time. We conduct an additional ablation study (Table 12), i.e., we compare with using all points in 2D bounding box for GPC. The experiment also shows the effectiveness of our design of DoubleClustering.

A.3.5. LEARNING PROCESS DETAILS FOR G_θ .

As mentioned in Section 3.2, we use the length of pseudo 3D bounding boxes to determine whether the object is *well-reconstructed*. This is a very simple yet effective metric, because we only need to find a good 3D box instead of its 3D surface in the object detection task. As mentioned in Section 3.2, G_θ can improve box size estimation accuracy. Here, we report size prediction error, as the average absolute relative error of length, width and height in Table 13.

	3D AP ₅	3D APH ₅	LET APL ₅₀	LET AP ₅₀
GPC	32.21	22.30	8.24	14.97
LPC+GPC	41.17	28.73	12.23	21.41

Table 12: Ablation study on DoubleClustering algorithm.

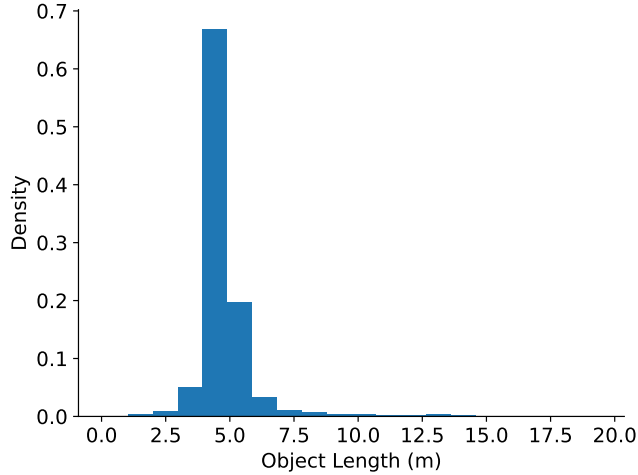


Figure 6: Statistical results of GT object length distribution.

Besides, in training G_θ , we do not simulate too large objects because we set a very loose length threshold. A vehicle whose length is too big ($>10\text{m}$) is very rare. According to the statistical results of GT (Fig. 6), it shows that less than 1% of objects have a length greater than 10m. We suppose that when the pseudo label is longer than 10m, it is likely that multiple objects have been incorrectly clustered into one cluster, resulting in a false positive. So we ignore this kind of cluster instead of learning a 3D box from it. As for the small pseudo box, we think it is a partially reconstructed object, and we can learn a full 3D box for it.

	3D AP ₅	3D APH ₅	LET APL ₅₀	LET AP ₅₀	Avg. Abs. Rel.
w/o G_θ	28.40	11.34	5.02	8.62	0.076
w/ G_θ	33.75	11.94	9.63	16.80	0.063

Table 13: Ablation study of G_θ . We also report results under the size prediction error metric.

A.3.6. ORIENTATION ERROR.

Our designs of orientation optimization (Sec. 3.1) and orientation loss can help orientation estimation. Besides APH metric, we also report more detailed orientation metrics. As for the orientation metrics, we report the average absolute relative error of orientation, defined as $\min(|\tilde{\theta} - \theta|, 2\pi - |\tilde{\theta} - \theta|)/\pi$, where $\tilde{\theta}$ and θ are the predicted heading and the ground truth heading. In Table 14, we discuss the main factors to influence the orientation estimation, (1) minimizing the sum of distance (r_y w/ d) and (2) orientation loss.

A.3.7. MOVING OBJECT FILTERING IN PSEUDO LABEL GENERATION.

The points on moving objects are mostly ignored in SfM. To further alleviate the effect of these points, we filter the object that has few points. We only keep the object cluster for more than $\theta = 100$ points. These objects may be dynamic objects that are not reconstructed well. The influence of this operation is ablated in Table 15.

	3D AP ₅	3D APH ₅	r_y Abs. Rel.
minAreaRectangle + MultiBin loss	33.75	11.94	0.205
r_y w/ d + MultiBin loss	38.39	24.33	0.099
r_y w/ d + Orientation loss	41.17	28.73	0.072

Table 14: **Impact of orientation optimization and loss design for orientation estimation.**

	3D AP ₅	3D APH ₅	LET APL ₅₀	LET AP ₅₀
ALL	36.03	24.92	9.27	16.38
Filter <100 points	41.17	28.73	12.23	21.41

Table 15: **Ablation study on few-point object filtering.**

A.3.8. PEDESTRIAN AND CYCLIST CATEGORIES.

Although we report the results of VEHICLE class in main paper, we would like to discuss the potential of BA²-Det for other categories as well. Other categories such as pedestrians and bicycles are primarily dynamic objects that would be affected by the moving object filtering operation in global scene reconstruction.

- As for 3D pseudo-label generation, "the points on moving objects are mostly ignored". That means 3D pseudo labels are rarely generated for pedestrians and cyclists due to their movement. (However, when they are static, such as waiting for a red light, the pseudo label can still be generated.) This is the natural shortage of SfM.
- Although lacking 3D pseudo labels, we can utilize the "generalization ability of depth from other objects" of the monocular 3D object detector. The other objects are mainly vehicles that are learned with 3D pseudo labels. We can generalize the depth of pedestrians/cyclists from the learned depth of vehicles. This generalization ability is because (1) Depth is the class-agnostic attribute of the object, and the network learns depth from the whole image. During the inference stage, the network can leverage the learned depth information of other vehicles in the same image to predict the depth of pedestrians and cyclists. (2) We train monocular 3D object detector with 2D assignment strategy. That means we will predict depth for all 2D objects, both vehicles and pedestrians/cyclists.

We show the object-level depth and orientation estimation accuracy in Table 16. As we can see, the average depth accuracy for pedestrians is no worse than vehicles. The training samples for the cyclist are too rare, and thus slightly affect the performance of the cyclist.

B. Qualitative Results

We show some qualitative results about 3D object detection and tracking (BA²-Det), open-set 3D object detection, and 2D MOT with auxiliary 3D representation (BA²-Det). For more qualitative results and video demos, please refer to the project page: <https://ba2det.site>.

Category	$\delta < 1.25 \uparrow$	$\delta < 1.25^2 \uparrow$	$\delta < 1.25^3 \uparrow$	Abs Rel \downarrow	Sq Rel \downarrow	RMSE \downarrow	RMSE log \downarrow	r_y Abs. Rel.
Car	0.993	0.995	0.996	0.093	0.558	3.367	0.198	0.0805
Pedestrian	0.981	0.992	0.994	0.055	0.292	3.086	0.104	0.0804
Cyclist	0.848	0.950	0.962	0.120	0.804	4.491	0.168	0.3737

Table 16: **Additional results on Pedestrian and Cyclist categories.** The middle columns show the object-level depth estimation results and the rightmost column shows the object-level orientation estimation results.

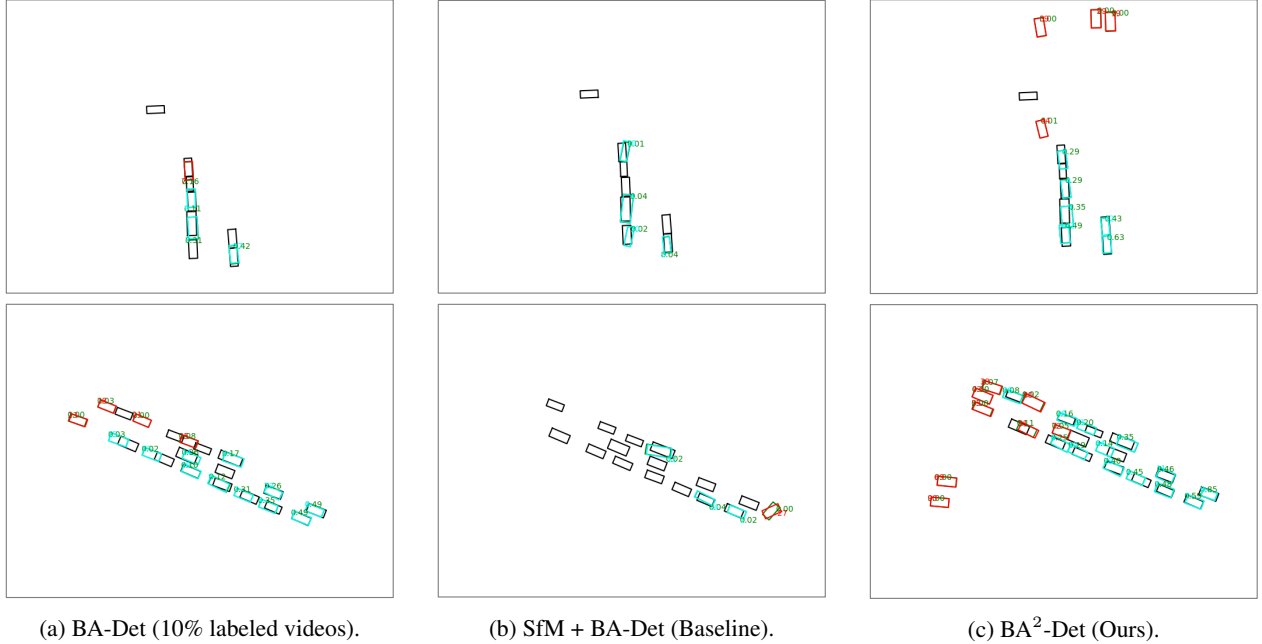


Figure 7: **Qualitative results of 3D object detection and tracking shown in BEV.** Black boxes are the ground truth, cyan boxes are the tracking results with id, green boxes are the detection results with scores, red boxes are the false positives.

B.1. 3D Object Detection and MOT Results on WOD

In Fig. 7, we show the qualitative results of BA-Det (trained with 10% labeled videos), the baseline method, and the proposed BA²-Det. Our method can achieve comparable performance with fully supervised BA-Det, and even better in some near cases. Compared with the baseline, a very obvious phenomenon is that our recall can be much better than the baseline method, mainly due to the iterative self-retraining design. The illustrations also show a typical failure case of BA²-Det that on a distance of about 75m, there are some false positives. This is because the 3D pseudo labels can be 0-200m and thus somewhat affects the training process. If the annotations include some farther objects, this problem may be alleviated.

C. Limitations and Future Work

We use 2D annotation to obtain pseudo 3D labels, and finally train a monocular 3D object detector with these pseudo labels. Similar to other monocular 3D detectors, we also encounter inherent issues such as inaccurate depth estimation and occlusion problems. The main contribution of this paper is proposing the use of weakly supervised methods to train a 3D detector. Compared to using 3D ground truth, our weakly supervised approach has the following limitations.

- The limitation of reconstructing videos: Our method relies on reconstruction to obtain pseudo labels, so it is limited by the usage conditions of SfM. It is difficult to achieve good reconstruction results when there is no ego-motion or when the camera undergoes severe movement in the dataset. The method doesn't work well for purely static video datasets. However, less than 5% of videos in the driving dataset do not meet the requirements, and we can use only pseudo labels with good reconstruction results to train the model. Therefore, this limitation can be greatly alleviated in driving scenarios. We also apply this method in more general scenes (Fig. 5), where most videos conform to the assumptions of this paper.
- The limitation of pseudo label quality: (1) Inaccurate orientation: Since many 3D clusters from the reconstructed scene are incomplete due to occlusion and self-occlusion, orientation estimation is more challenging than 3D location and 3D shape estimation. In section 3.2, we try our best to alleviate this problem. However, it still affects the performance and becomes an open problem. (2) Big cluster containing more than one object: When some objects are side-by-side, like in a parking lot, the clustering algorithm may output a big object cluster containing more than one object. We filter this

kind of cluster by 3D shape threshold. In the future, we will improve the clustering algorithm to solve this problem. (3) Time-consuming iteratively self-retraining: Although iteratively self-retraining can improve performance a lot, it takes more than double the training time. We will try to decrease the time cost and keep the performance in the future work.

D. Broader Impacts

This paper presents work whose goal is to advance the field of Machine Learning. There are many potential societal consequences of our work, none which we feel must be specifically highlighted here.